

Integrated-optics-based swept-source optical coherence tomography

V. Duc Nguyen,^{1,*} N. Weiss,¹ W. Beeker,² M. Hoekman,² A. Leinse,² R. G. Heideman,²
T. G. van Leeuwen,¹ and J. Kalkman¹

¹Biomedical Engineering & Physics, Academic Medical Center, University of Amsterdam, P.O. Box 22700, Amsterdam 1100 DE, The Netherlands

²LioniX BV, P.O. Box 456, Enschede 7500 AL, The Netherlands

*Corresponding author: d.v.nguyen@amc.uva.nl

Received August 31, 2012; accepted October 1, 2012;

posted October 10, 2012 (Doc. ID 175330); published November 16, 2012

We designed, fabricated, and characterized an integrated-optics-based swept-source optical coherence tomography (SS-OCT) system in TriPleX technology. An external 1300 nm swept source is coupled to the chip, which contains waveguide structures for interferometric depth ranging and balanced detection. The complete OCT chip has a footprint of $0.4 \text{ cm} \times 1.8 \text{ cm}$. Light from the chip is focused onto the sample using an aspheric lens; the lateral resolution is $21 \pm 1 \mu\text{m}$. OCT measurements, performed with a moveable mirror, demonstrate a sensitivity of -80 dB and imaging up to the maximum depth of 5.09 mm. Corrected for dispersion, the measured OCT axial resolution of $12.7 \pm 0.5 \mu\text{m}$ is in good agreement with the bandwidth limited resolution. Finally, we demonstrate cross-sectional OCT imaging of a multilayered tissue phantom over the whole depth range with the integrated-optics-based SS-OCT system. © 2012 Optical Society of America

OCIS codes: 100.3175, 170.4500, 170.3880, 230.3120, 130.3990.

Optical coherence tomography (OCT) is an interferometric imaging technique that can make high-resolution images up to a few millimeters deep [1]. Currently, OCT has its main applications in ophthalmology and intravascular imaging. Still, the widespread use of OCT in medicine and in other application areas, such as forensics, biometrics, and process control, is held back by its high costs and its large form factor. Integrated optics has the potential to make OCT devices and components significantly smaller, more functional, and more cost efficient [2].

Recently, we designed and fabricated integrated-optics components for OCT, such as elliptical couplers [3] and AWG spectrometers [4,5], and demonstrated their use in spectral-domain OCT.

Compared to spectral-domain OCT, swept-source OCT (SS-OCT) has the advantage of a simpler optical design and larger imaging depth [6]. Recently, Yurtsever *et al.* [7] presented an integrated-optics interferometer in silicon on insulator and performed SS-OCT depth ranging. Yet, the measured OCT axial resolution was not bandwidth limited and the signal-to-noise ratio (SNR) was too low for imaging of turbid media. In this work, we demonstrate the design, fabrication, and characterization of an integrated-optics-based SS-OCT system and demonstrate cross-sectional OCT imaging of a multilayered tissue phantom.

An optical chip containing waveguides is produced in TriPleX technology platform [8] and the waveguide geometry is a single strip Si_3N_4 of 50 nm height and $3.4 \mu\text{m}$ width. The top and bottom SiO_2 cladding layers are $8 \mu\text{m}$ thick. Waveguides operate in single mode at 1300 nm wavelength and have a minimum bending loss for TE polarization. At the end facets of the chip waveguides are tapered down to $1 \mu\text{m}$ to match the mode field diameter ($9.2 \mu\text{m}$) of a standard single mode fiber (SMF-28) to achieve optimal fiber-to-chip coupling. Waveguide splitters are made using directional couplers (DCs). A schematic of the on-chip waveguide layout and the

experimental setup is shown in Fig. 1(a). The chip contains a Michelson interferometer, sample arm, reference arm, and two identical DCs for light splitting and balanced detection. The optical path length of the reference arm is chosen such that the zero delay point is 6.9 mm away from the edge of the chip. A single OCT chip is only $0.4 \text{ cm} \times 1.8 \text{ cm}$.

The integrated-optics-based SS-OCT is compared to a home-built bulk optics SS-OCT system shown in Fig. 1(b). Both integrated-optics-based and bulk SS-OCT systems use an Axsun swept source with a center wavelength of 1312 nm, 20.9 mW output power, 50 kHz repetition rate, and $\sim 50\%$ duty cycle. The start of the wavelength sweep is detected using the light reflected from a fiber Bragg grating (FBG) at $\lambda = 1266 \text{ nm}$ (OE Land). For both systems the interference spectrum is detected on a balanced photo detector (Thorlabs, PDB450C). The signal from the FBG triggers a 500 MHz digitizer (Alazar Tech, ATS9350) that acquires

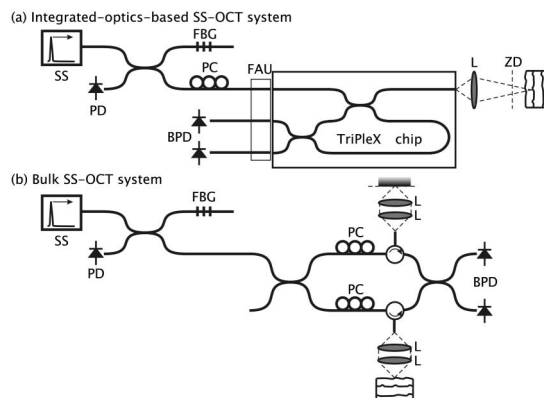


Fig. 1. Schematic of the experimental setup used for (a) the integrated-optics-based SS-OCT and (b) the bulk SS-OCT system. SS, swept source; FBG, fiber Bragg grating; FAU, fiber array unit; PC, polarization controller; BPD, balanced photo detector; L, lens; PD, photodiode; and ZD, zero delay.

1088 samples using the Axsun k clock as an external clock signal. The 1088 clock cycles are equivalent to 92 nm of optical bandwidth corresponding to a maximum image depth of $z_{\max} = 5.09$ mm. OCT depth scans are generated by Fourier transformation of the interference spectrum. To correct for dispersion differences between the sample and reference arm, the spectrum is resampled using a second-order dispersion correction in the wavevector versus frequency relation [9], while keeping the total optical bandwidth fixed.

The bulk SS-OCT system is based on a 90:10 fiber optics splitter with 90% of the light going to the sample arm and 10% going to the reference arm. The two arms of the interferometer are fully symmetric to avoid any dispersion mismatch. Light from the sample and reference arm are mixed and split by a 50:50 splitter for balanced detection.

In the integrated-optics-based SS-OCT system, light from the swept source is coupled into the chip via a fiber array unit (FAU) based on SMF-28 fibers with 127 μm pitch. A polarization controller is placed on the input fiber of the FAU to couple TE polarized light into the chip. In the chip, light is split into sample and reference arm by the first DC. In the sample arm, light from the waveguide is focused onto the sample by an aspheric lens (Geltech 355200). Back-reflected light from the sample goes again through the first DC and is recombined with light from the reference arm in the second DC. There it is split and coupled into two fibers of the FAU that are connected to the balanced detector. In all measurements, unless indicated otherwise, the focus position is set to 0.5 mm after the zero delay point. For this focus position the measured NA of the lens is 0.020 ± 0.001 , corresponding to a lateral resolution of 21 ± 1 μm .

The measured splitting ratio of the DC (data not shown) is 80:20 at the center of the wavelength band (1312 nm) with 80% of the light going to the bar port and 20% of the light going to the cross port. The splitting ratio varies from 90:10 (1266 nm) to 75:25 (1358 nm) over the source spectrum. Ideally, both DCs split the light in a ratio of 50:50 independent of wavelength; however, due to fabrication errors this ideal splitting ratio was not reached.

Figure 2 shows the OCT signal in depth measured for a moveable mirror in the sample arm. The raw OCT signal in Fig. 2(a) shows poor axial OCT resolution for all depths. After dispersion correction at every depth the OCT signal increases and the axial resolution improves [Fig. 2(b), same vertical scale as in Fig. 2(a)]. We measured the back-reflected light intensity from the mirror in the sample arm. After correcting for the OCT signal dependence on field and correcting for the SS-OCT system sensitivity roll-off in depth, we obtain a signal decrease as shown with the solid curve in Fig. 2(b). As can be observed, the decrease of the OCT signal in depth is well described by the combined effects of SS-OCT system sensitivity roll-off in depth and lens focusing. The OCT axial resolution is determined by taking the full width at half-maximum of the OCT signals in Figs. 2(a) and 2(b) and is shown in Fig. 2(c). For all depths the dispersion mismatch between the waveguide material and air can be fully corrected. The measured average axial resolution of 12.7 ± 0.5 μm is in excellent agreement with the bandwidth limited axial resolution of 12.5 μm , which

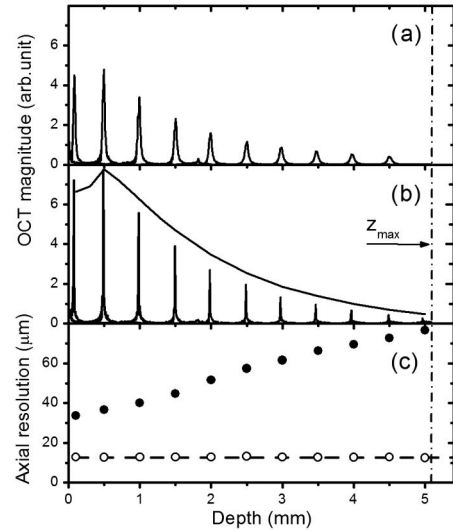


Fig. 2. Measured OCT signal in depth for a mirror in the sample arm. (a) OCT signal without dispersion correction and (b) OCT signal with dispersion correction. The solid curve indicates the SS-OCT signal drop due to system sensitivity and lens focusing. (c) Measured OCT axial resolution before (filled circles) and after (open circles) dispersion correction. The dashed line indicates the bandwidth limited OCT axial resolution and the vertical dashed line indicates the maximum imaging depth (z_{\max}).

is calculated from the reference arm spectrum measured on one port of the balanced detector [4].

The OCT sensitivity is measured with the integrated-optics-based SS-OCT using a glass plate as a reflector with 4% reflectivity in the sample arm. The measured SNR at a depth of 500 μm is 66 dB. This is 3 dB worse than measured with the bulk optics OCT system (SNR = 69 dB) using the same digitizer acquisition settings, sample, depth location, reference arm power, and sample arm power. From the glass reflectivity and the measured SNR we calculate the sensitivity of the integrated-optics-based SS-OCT to be -80 dB.

As a demonstration of OCT imaging using the integrated-optics-based SS-OCT system, images of a layered tissue phantom are obtained by sample scanning. The tissue phantom consists of three layers of scattering medium ($\mu_s = 4$ mm^{-1} , refractive index $n = 1.41$) [4] interleaved with nonscattering tape. Figure 3 shows OCT

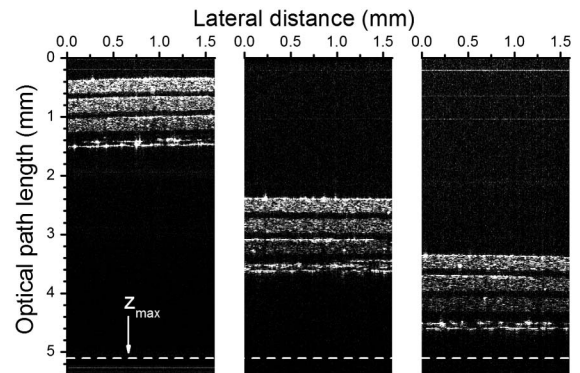


Fig. 3. OCT images of the tissue phantom measured with the integrated-optics-based SS-OCT system for three different sample depth locations.

images of the tissue phantom at three different depth locations. For each depth location the dispersion correction is optimized and the focus position adjusted (500, 2500, and 3500 μm , for increasing depth location). All three scattering layers can be clearly observed at the three depth locations.

The measured -80 dB integrated-optics-based SS-OCT sensitivity is affected by the following issues. (1) A measured 1.5 dB fiber-to-chip coupling loss and a 3.5 dB chip-to-fiber coupling loss, which is mainly due to FAU-to-chip misalignment and small offsets between the fiber and waveguide cores (typically 0.5 μm). In case of perfect alignment, fiber (round core) to waveguide (rectangular core) coupling loss is calculated to be 0.4 dB. (2) Unlike the bulk optics SS-OCT system, which collects most of the back-reflected light from the sample arm via a circulator, ideally, an integrated-optics-based SS-OCT with an 80:20 DC can only collect 16% of the back-reflected light from the sample (maximum 25% with a 50:50 DC), which leads to a 6.9 dB reduction in SNR compared to the bulk system. However, this issue can possibly be solved by incorporating an integrated-optics circulator [10] into the chip design. (3) The 80:20 splitting ratio is not constant over the entire bandwidth of the DCs, resulting in suboptimal balanced detection, which leads to a reduction in sensitivity [11]. We measured on the bulk SS-OCT system a 5 dB noise increase due to operating the digitizer at a higher voltage setting, necessary to handle the noninterferometric variation of the signal over the spectrum due to nonideal balancing. However, we expect that these issues can be solved with the design and fabrication of a 50:50 wavelength-flattened DC [12]. Considering the aforementioned loss processes we estimate that the performance of the integrated-optics-based SS-OCT system can be improved by 10–15 dB, bringing the performance of integrated-optics-based SS-OCT systems close to that of commercially available bulk SS-OCT systems.

In conclusion, we demonstrated the design and characterization of a 1300 nm integrated-optics-based SS-OCT.

Imaging of a layered tissue phantom with the integrated-optics-based SS-OCT system demonstrates the feasibility of integrated-optics-based SS-OCT imaging.

This work was supported by the Smart Mix Program of the Netherlands Ministry of Economic Affairs and the Netherlands Ministry of Education, Culture and Science and the IOP Photonic Devices program managed by the Technology Foundation STW and Agentschap NL.

References

1. D. Huang, E. A. Swanson, C. P. Lin, J. S. Schuman, W. G. Stinson, W. Chang, M. R. Hee, T. Flotte, K. Gregory, C. A. Puliafito, and J. G. Fujimoto, *Science* **254**, 1178 (1991).
2. D. D. Culemann, A. Knuettel, and E. Voges, *IEEE J. Sel. Top. Quantum Electron.* **6**, 730 (2000).
3. V. D. Nguyen, N. Ismail, F. Sun, K. Wörhoff, T. G. van Leeuwen, and J. Kalkman, *J. Lightwave Technol.* **28**, 2836 (2010).
4. V. D. Nguyen, B. I. Akca, K. Wörhoff, R. M. de Ridder, M. Pollnau, T. G. van Leeuwen, and J. Kalkman, *Opt. Lett.* **36**, 1293 (2011).
5. B. I. Akca, V. D. Nguyen, J. Kalkman, N. Ismail, G. Sengo, F. Sun, A. Driessen, T. G. van Leeuwen, M. Pollnau, K. Wörhoff, and R. M. de Ridder, *IEEE J. Sel. Top. Quantum Electron.* **18**, 1223 (2012).
6. M. A. Choma, M. V. Sarunic, C. Yang, and J. A. Izatt, *Opt. Express* **11**, 2183 (2003).
7. G. Yurtsever, K. Komorowska, and R. Baets, *Proc. SPIE* **8091**, 80910T (2011).
8. J. F. Bauters, M. J. Heck, D. John, D. Dai, M. C. Tien, J. S. Barton, A. Leinse, R. G. Heideman, D. J. Blumenthal, and J. E. Bowers, *Opt. Express* **19**, 3163 (2011).
9. A. Kohlhaas, C. Fromchen, and E. Brinkmeyer, *J. Lightwave Technol.* **9**, 1493 (1991).
10. N. Sugimoto, T. Shintaku, A. Tate, H. Terui, M. Shimokozono, E. Kubota, M. Ishii, and Y. Inoue, *IEEE Photon. Technol. Lett.* **11**, 355 (1999).
11. Y. Chen, D. M. de Bruin, C. Kerbage, and J. F. de Boer, *Opt. Express* **15**, 16390 (2007).
12. A. Takagi, K. Jinguji, and M. Kawachi, *IEEE J. Sel. Top. Quantum Electron.* **28**, 848 (1992).